Period- and Branch-Calibrated TI-PLM Holography for Selective Industrial LiDAR

Adnan Asghar[1,*] and Noah Oliver[1]

[1] University of Alberta, Edmonton, Canada
* Correspondence: adnanasghar14041985@gmail.com

Abstract: Non-mechanical compact beam steering is essential for industrial LiDAR, robotic inspection, optical metrology, and safety monitoring because in most cases, the applications require illumination of specific regions and not a raster scanning over the whole scene with uniform resolution. The Texas Instruments phase light modulator (TI-PLM) provides a solution to the problem via a MEMS-based holographic steering based on phase only. However, the TI-PLM controller is forced to operate on a grid of mirrors, 10.8 µm pixel pitch, and 16 nonlinear phase states instead of a continuous phase ramp. In this research, we consider the reliability of multi-region steering using the TI-PLM controlled by a command protocol that depends on a calibration table containing information about the period-dependent loss of efficiency, phase-mismatch sensitivity due to rotation, and different diffraction power between two regions of interest. The quantitative calibration information includes weak periods of normalized diffraction efficiency at $r = 3$, 5.5, 6.5, and 7.5, the recovery of diffraction efficiency to 0.42 from 0.37 due to small in-plane rotation at $r = 3$, and diffraction efficiencies of two regions in symmetric and asymmetric hologram configurations. For a particular command, the steering request can be sent to the device unmodified, rotated, weighted by the branching parameter, or time-separated depending on the diffraction efficiency difference. The analysis demonstrates that the rotation-sensitive $r = 3$ period provides a 13.5% relative recovery without any hardware changes. Asymmetric two-region steering commands should incorporate amplitude buffer of 17.1% and 20.8% at a weak-branch condition in case of complex-field addition. Therefore, the TI-PLM guidance scheme is appropriate for the use in multi-regional industries LiDAR systems only if the issue of beam positioning is considered a control process, not a geometrical mapping from the required angle to the hologram period.

Keywords: TI-PLM; MEMS phase light modulator; LiDAR; computer-generated holography; beam steering; diffraction efficiency; industrial sensing; region-of-interest illumination; smart manufacturing; optical calibration

Citation: Adnan Asghar and Noah Oliver. 2022. Period- and Branch-Calibrated TI-PLM Holography for Selective Industrial LiDAR. *TK Techforum Journal (ThyssenKrupp Techforum)* 2022(1): 58–75.

Received: October-14-2022
Accepted: November-29-2022
Published: December-30-2022

1. Introduction

There are several use cases for industrial LiDAR systems and machine-vision platforms where attention is limited, time is precious, and optical power has to go only where there is decision value. There is a difference between the sampling behavior required for scanning a pallet edge by a robot, the motion of a collaboratively operating robotic arm next to a person, metrology of a narrow tolerance feature, and guidance of an AGV through an aisle. Each scenario requires fast reorientation of the beam to those parts of the scene that bear immediate importance for the particular application. This means that the steered component plays a crucial role for how often, how powerful, and predictably the measurements take place at revisiting the zone of interest. Conventional mechanically driven systems still offer valuable capabilities in terms of angular range and apertures sizes; however, they have several inherent drawbacks in terms of inertia, wear, and vibrations making them incompatible with the high cycle-rate requirement for embedded sensing. Consequently, solid-state or MEMS methods have been gaining increasing importance in LiDAR and

automated industry due to their ability to reduce the mass and enable the integration of digital circuits [1–6].

Wavefront-controlled programmability provides a flexible basis for non-mechanical beam steering. One approach is to create an arbitrary far-field pattern using computer-generated holography, and then use a phase shifter to steer an optical beam by deflecting it with a macroscopic mirror movement. It draws its origins from classic kinoform and binary holography concepts, where a phase or amplitude filter transforms an input wave into a designated diffraction pattern [7,8,10]. The technique was furthered by phase retrieval and hologram design, allowing the practical realization of highly efficient far-field patterns through limited pixel arrays [11–13]. Modern applications include dynamic optical manipulation, adaptive microscopy, diffractive display technologies, structured illumination, and beam steering modules [14–17]. Industrial LiDAR systems have been interested in holographic beam steering due to the ability to steer, split, or focus beams on many points of interest as long as the phase function approximates the desired optical function [18].

The physical problem lies in the fact that real SLMs are not mathematical continua. The pitches are discrete, the response phase is not necessarily linear, and the fill factors and diffractive orders are specific to particular devices. Liquid-crystal SLMs exhibit excellent phase modulation capability but suffer from insufficient response time to enable fast scene sampling, whereas digital micromirror SLMs can be switched quickly but are typically limited by their modulation schemes, being either based on the amplitude scheme or the binary phase one, unless some optical tricks are involved [19–23]. Silicon photonics optical phased array provides another path toward achieving chip-level beam steering, which shows remarkable results for LiDAR applications, but at the same time raises concerns about grating lobe suppression, aperture scalability, thermal tunability, and alias-free angular scanning [24–26]. MEMS phase light modulator is a compromise solution since it can benefit from modern digital microfabrication, phase-only operation, and moderate response times, making use of known digital light processing techniques [27–30].

A second body of literature is pertinent inasmuch as an industrial optical instrument does not generally fail solely because of optical element malfunction. It fails because there is an independence assumption made between a steering command, detector integration time, surface reflectance, and control decision while in reality they all interrelate in the measurement process. Literature review on automotive and robotic LiDAR indicates that range and object estimation accuracy depends on the combination of scanning optics, aperture size of receiver, signal processing and dynamics of the scene [2–4]. An additional relationship between parameters appears in the case of holographic steering where far-field intensity is a function of the digital phase realization. Even if a command is geometrically accurate, it will not result in a precise measurement if it results in low diffraction efficiency for the desired hologram order. This explains why the TI-PLM operation is addressed here from the perspective of calibration. The phase bitmap output from the steering controller should be augmented with an estimate of expected efficiency and power branch allocation.

Computer-generated holography provides a classical example illustrating the interpretation proposed above. Early studies highlighted the fact that there were plenty of phase functions that led to similar far-field intensity distributions [11,12]. Practical hologram design was always a trade-off between diffraction efficiency, intensity uniformity, phase noise, and computation cost [13]. Later on, the same trade-off has been particularly noticeable in optical trapping [15] and microscopy [16,17], both of which required multiple spots. The industrial application of LiDAR also brings up the question of trade-off between diffraction efficiency and power uniformity but the terminology used is quite different. A weak spot in this case is no longer a trapped particle; rather, it refers to a surface whose return signal may have a strong effect on machine motion, part inspection, or obstacle detection.

In the current discussion, the relevance of the TI phase light modulator lies in its conversion of a MEMS mirror array from intensity modulation into phase modulation. The TI-PLM can be instructed to create a saw-tooth profile in case of single point steering as well as multi-point phase maps in case of multiple beams. However, the very manufacturing

capabilities that make the TI-PLM attractive bring their own challenges to the system control problem. An ideal hologram written onto a continuous phase gradient is not applicable here since the TI-PLM array only offers up to 16 discrete phase steps with a spacing of 10.8 µm. As a result, some normalized grating periods lead to more efficient performance of the TI-PLM while others create known valleys for the measured efficiency function. An angle-based controller would then drive particular holograms into known inefficient areas, but a rotated basis and a reassignment of time could improve the efficiency [31,32].

In this paper, we address the controller implications of the findings. In other words, we wonder whether an industrial LiDAR system can use a TI-PLM as a multi-point steering engine provided that its hologram creation procedure follows a pre-calibrated ledger rather than an open-loop angle command. We understand reliability as the ability to avoid low efficiency due to a bad grating period, rotate the basis in order to restore at least a portion of the loss, and balance branches of the two beams of interest.

1.1. Device Evidence and Research Goal

The optical performance of the TI-PLM can be examined starting from the mirror cell upwards. Each mirror is activated electrostatically and causes an individual phase retardation of the outgoing wavefront. In contrast to a liquid crystal phase modulator whose voltage-to-phase response can be calibrated across a rather smoothly changing analog function, the body of evidence for the TI-PLM discussed here comprises 16 available phase states caused by nonlinear mirror deflection. The mirror cell size is 10.8 µm, so that the blazed period in terms of normalized pixels cannot be considered as a mere theoretical value, but describes the number of cells corresponding to one period of the phase ramp. For a small period value, a small number of sampling points in each cycle 2π of the blazed phase will make the effect of a phase ramp less uniform. However, if the period grows, then the number of phase steps used for its discretization increases.

In the experimental setup of Figure 1, the TI-PLM lies between the beam conditioning optics and far-field viewing, and the configuration represents the assumptions made in all the steering experiments described. The picture is relevant since it indicates that the modulator chip is never studied in isolation, but rather in the role of the phase-addressing component of a LiDAR beam train. In other words, commanding success hinges on the entire chain, starting from the incoming beam to holographic diffraction to the final power detected in the chosen region.

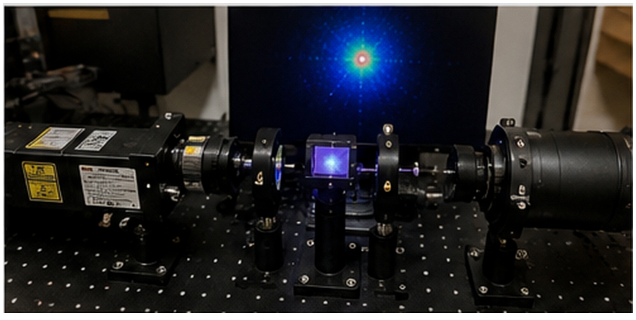

Figure 1. Selective TI-PLM optical bench.

The physical scale of the steering problem is determined by the mirror surface shown in Figure 2. The 10.8 µm cell pitch defines the sampling of any commanded phase ramp while the fact that the micromirror array is not ideal but has a limited extent means that there will always be discretization of a perfect continuous ramp when implemented optically. These two factors form the very basis of the research project. A hologram control system using just the commanded angles would ignore the physical manifestation of the ramp, while a calibration database could take the intended effect of drawing a certain ramp on a certain lattice into account.

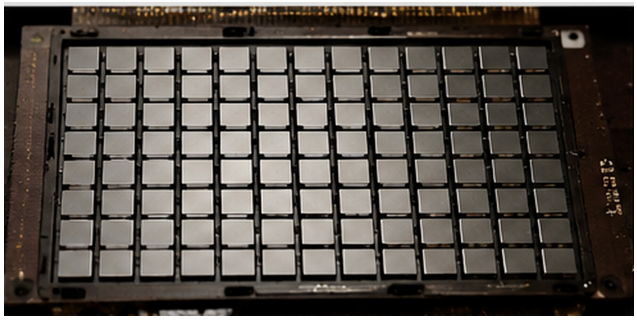

Figure 2. TI-PLM micromirror surface.

It becomes clear from Figure 3 that the assumption of equidistant quantization is invalid for phase readout. In the case of a staircase, quantization error would still be consistent and easy to approximate. However, the TI-PLM's phase state sequence is not as simple because the distance between phase states changes and results in non-uniform far-field rings for the 16 addressable states. Thus, it is necessary to account for the way in which the desired sawtooth profile matches the available state sequence within a period. The difference in performance may be considerable enough to justify using a period-specific calibration ledger rather than a generic phrase like "16-level phase modulator."

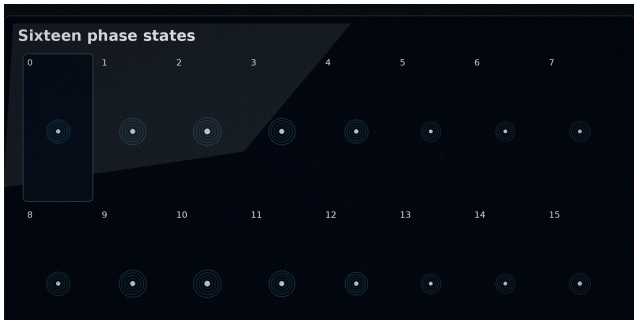

Figure 3. Sixteen phase-state readout.

As such, the research goal is clear given the above device properties. A command to multi-region industrial LiDAR can be assumed safe for dispatch only if the power of the optical radiation at each target region exceeds the sensing margin determined by the detector threshold and exposure time given the reflectance conditions. For cases in which a period happens to belong to a weak range, the steering engine should generate a rotated hologram. In the case of commanding multiple regions with one hologram, a weaker branch should be weighted prior to acceptance of the command. Otherwise, the command should be split into several temporal fragments. This is how one defines a period-sensitive control policy rather than a simple hologram generator algorithm. The analysis will make use of the documented TI-PLM values: weak periods occur near $r = 3$, 5.5, 6.5, and 7.5. Rotation-based hologram recovery takes place near $r = 3$ within 0.37–0.42 range. Multi-region efficiencies were found for 3 ROI pairs [32].

Table 1's entries turn the characterization of devices into a language for control. The relation of the measure or structure to the decision made by the steering engine is important because the same hardware can be used for steering in a fundamentally different way. On the one hand, a specified angle can be encoded in a hologram and used to steer the device. On the other hand, the angle can be assessed based on a calibration table that indicates whether the device can generate enough optical power under the specified encoding. The latter mode is studied herein because it brings industrial sensing closer to the problem at hand, where the optical risk of a command needs to be made explicit prior to illumination.

Table 1. Calibration variables used for command screening.

Ledger entry	Quantitative basis	Control meaning
Pixel pitch	$D = 10.8\,\mu\text{m}$	Converts a commanded normalized period into a sampled phase ramp on the mirror lattice.
Phase alphabet	16 nonlinear phase states	Determines whether the ideal sawtooth ramp is represented by a uniform or locally biased phase sequence.
Weak periods	Valleys near $r = 3$, 5.5, 6.5, and 7.5	Marks periods that require caution, basis testing, or temporal separation when power margin is limited.
Rotation margin	$\eta = 0.37$ to 0.42 at $r = 3$	Shows that part of the loss can be recovered by changing the coordinate basis without changing the optical head.
Two-ROI efficiencies	Measured paired-region data for layouts (a), (b), and (c)	Supplies branch-specific efficiency estimates for amplitude weighting and dispatch decisions.

2. Hologram Synthesis Conditional Upon Calibration

Steering commands start with the specified far-field direction or regions of interest. When there is a single point, the corresponding continuous target can be expressed using a blazed phase profile, the period of which defines the steering angle. In the case of multiple points, the target field is a coherent superposition of components related to different regions. While the continuous-field description can be helpful in that it represents the target optical function, it cannot provide a means to test whether this function can be represented in a compact way by a TI-PLM. Therefore, a representation stage is required before a hologram is created for a given command.

Let $\phi(x, y; r)$ stand for the continuous phase profile corresponding to the steering period r. If the target phase profile has been converted to the TI-PLM phase alphabet with respect to a certain pixel p, let θ_p represent the associated device phase state. Assuming a small basis rotation α, the phase profile can be evaluated in the rotated coordinate system. The difference between the target phase profile and the one corresponding to the implemented phase is expressed via the RMS phase error,

$$\sigma_{\text{rms}}(\alpha; r) = \left[\frac{1}{ND} \sum_{p=0}^{N-1} \int_{pD}^{(p+1)D} \left(\phi_\alpha(x) - \theta_p\right)^2 dx \right]^{1/2}, \tag{1}$$

where D is the mirror pitch and N is the number of pixels during the effective steering period. Such an equation does not represent a complete model for the propagation of light. This equation represents a predictor of the quality of the representation. A small value indicates that the state of the device changes in accordance with the required ramp; a large value suggests that the phase lattice may transmit energy outside the required diffraction order.

Selection of the appropriate basis for the control algorithm is performed by finding an optimal rotation of a limited number of candidates.

$$\alpha^\star(r) = \arg\min_{\alpha \in \mathcal{A}} \sigma_{\text{rms}}(\alpha; r), \tag{2}$$

where $\mathcal{A}$ denotes a finite set of rotations that are calculated beforehand. The reason why we consider only a finite set of rotations lies in our desire for efficient computation. An industrial controller should take some time to compute actions. In addition, the controller's operation must be repeatable, so any broad optimization performed for every pulse or frame is unacceptable. All we need is a lookup table or a limited search near the zero rotation

command that allows us to recover from bad times. Thus, we use rotation as an embedded correction rather than a geometrical flourish.

To construct a phase map for a multiple-region command, we will combine weighted components of the map,

$$\Phi(x,y) = \arg\left[\sum_{k=1}^{K} w_k \exp(j\phi_k(R_{\alpha^\star}[x,y]))\right], \tag{3}$$

where $R_{\alpha^\star}$ is the chosen coordinate transform, ϕ_k is the phase mask for target k, and w_k is the nonnegative branch weight. This phase function is created by taking the argument of the complex field. In general, complex-field addition operations are commonly used in phase-only holograms and optical tweezers; however, this problem statement is more restrictive than that in those cases since the weights chosen will be to counteract the measured branch efficiency for the particular two-region TI-PLM steer [19,20,33].

This branch-weighting rule can be determined using efficiency calibration information. Suppose the proportion of power delivered to target k should be ρ_k, and suppose the expected branch efficiency without branch weights is $\hat{\eta}_k$. Then a useful amplitude weighting rule is

$$w_k = \frac{\sqrt{\rho_k / \max(\hat{\eta}_k, \varepsilon)}}{\left(\sum_{m=1}^{K} \rho_m / \max(\hat{\eta}_m, \varepsilon)\right)^{1/2}}, \tag{4}$$

where ε prevents division by zero in an inadmissible branch. For equal-priority two-region steering, the relative buffer for a weaker second region becomes

$$\gamma = \frac{w_2}{w_1} = \sqrt{\frac{\hat{\eta}_1}{\hat{\eta}_2}}. \tag{5}$$

Square root relationship is key in the sense that it translates intensity efficiency into field amplitude. For the case where the branch measures lower intensity, there would be no need to increase field proportionately to intensity; rather, it should have been done in proportion to the square root of efficiency.

Figure 4 illustrates a ledger display that must be interpreted as a control log rather than a standard flow chart. A region of interest is entered into the controller, the phase lookup restricts the command to the TI-PLM alphabet, rotation of the basis occurs if the ledger suggests a low-efficiency period, and branch weights are computed only after the efficiency of a likely single branch is evaluated. Such sequencing ensures proper handling of a frequent mistake in multiple regions hologram creation; compensation of a branch before the evaluation of its efficiency state. In industry LiDAR modules, such sequence allows tracking. If the command or temporal splitting of a command is rejected, the cause is known as a predetermined efficiency threshold, not as the undefined problem in the optics.

Figure 4. Calibration ledger display.

The dispatching decision can be formulated as a criterion of admissibility. Given $\eta_{\min}$ as the lowest efficiency level of delivery allowed for a region at the current exposure level and detector margins and $I_{\max}$ as the highest level of imbalance allowed for illumination with equal priority between two regions, direct dispatch of a single-region command is allowed when the calibrated efficiency with regard to the selected basis satisfies $\hat{\eta}(r, \alpha^{\star}) \geq \eta_{\min}$. Direct dispatch of a two-region command is allowed when the weighted efficiency estimates for both branches are greater than $\eta_{\min}$ and the imbalance index is below $I_{\max}$. The imbalance index used here is

$$I = \frac{|\eta_1 - \eta_2|}{\eta_1 + \eta_2}. \tag{6}$$

This metric is straightforward, bound by zero and one, and easily interpretable. A close proximity to zero suggests equal power distribution among the branches; if it has a large value, then one of the branches is clearly delivering significantly less power than the other branches. From the perspective of monitoring safety and measuring dimensions, such a branch inequity becomes as important as overall efficiency of optical transmission.

3. Quantitative Results and Discussion

The actual period-efficiency profile highlights the reason why the steering cannot be captured by a monotone relationship between the grating period and its efficiency of optical power transmission. Ideally, the first diffraction mode of the blazed grating would be highly efficient for a wide range of periods. A phase ramp having sixteen levels would have a well-known penalty due to the quantization effect but would show smooth response. However, both TI-PLM-constrained and experimental results deviate from the ideal profile: there are distinct regions of low efficiency located around $r = 3$, 5.5, 6.5, and 7.5 [31,32].

The first practical use of the period-efficiency record in Figure 5 arises immediately. A command close to a weak period is not just another routine steering command; it is an inherently risky command whose optical performance depends directly on representation error rather than just on required steering geometry. Not all commands are out of the question, but the controller needs to consider if there exists an alternative command representation, perhaps just a slight rotation of the basis itself, which would allow the command to move the device out of the period neighborhood in question. Thus, the period record takes us beyond device calibration into command filtering.

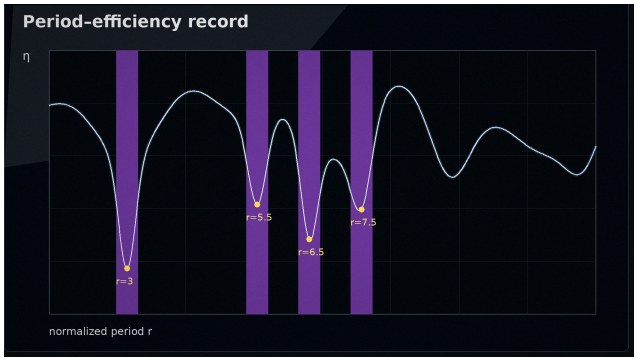

Figure 5. Period-efficiency record.

The impact of the weak periods becomes clear once we consider the steering module in the context of the ranging process as a whole. If the efficiency in first order is decreased for a particular steering module, then the number of photons delivered to the field point of interest before accounting for the effects of reflectance, collection, and noise penalties is also decreased. In a highly reflective laboratory target environment, even an intermediate efficiency loss will be sufficient to yield adequate range performance. However, in a lower reflectivity environment, such as a warehouse, factory cell, or outdoors in a loading area, an efficiency dip will contribute to the overall reduction in range due to oblique incidence, dust, or background. The period map must henceforth be seen as a derating table that

operates at an earlier stage. The table informs the controller how much optical margin has been spent by the steering action prior to measuring the scene.

Secondly, the valleys are selective. The fact that they occur at multiple normalized periods implies structural interactions, not mere experimental noise. This is in accordance with the diffraction theory of quantized and pixelated phase devices, whereby energy will be confined within the target order only if the sampled phase profile has sufficiently small error [9,10] in approximating the target wavefront. They also illustrate why reporting one value of efficiency is inadequate. While an industrial data sheet might provide an estimate of the overall efficiency, the efficiency at each particular normalized period must be used by the steering controller. A LiDAR system alternating between high-efficiency and low-efficiency periods would yield signals of varying ranges or angles even if the power of the emitted laser was kept constant. Without accounting for this variation, a change in signal could be mistakenly attributed to changing reflection off the target unless the optical margin is reported by the steering controller.

For the case of $r = 3$ where recovery was seen, the measurement reveals that the diffraction efficiency rises from 0.37 to 0.42 upon rotating the phase basis slightly within the plane. An absolute increase of 0.05 efficiency units corresponds to a relative recovery of $(0.42 - 0.37)/0.37 = 0.135$, or 13.5% recovery. Neither the change in the mirror hardware, laser wavelength, nor aperture size led to such improvement. What did help was reprogramming the representation of the desired phase ramp on the lattice. This is a key point in the argument since it demonstrates that device calibration can be translated into a true command margin.

The unrotated $r = 3$ pattern in Figure 6 is the weak-period condition prior to basis correction, when the first-order efficiency is measured at 0.37. The bright central point persists, but the speckling around indicates that there are still some optical energies left over which do not belong to the required order. Visually speaking, this stage is associated with a good geometrically valid, yet marginally useful, range-dependent control signal.

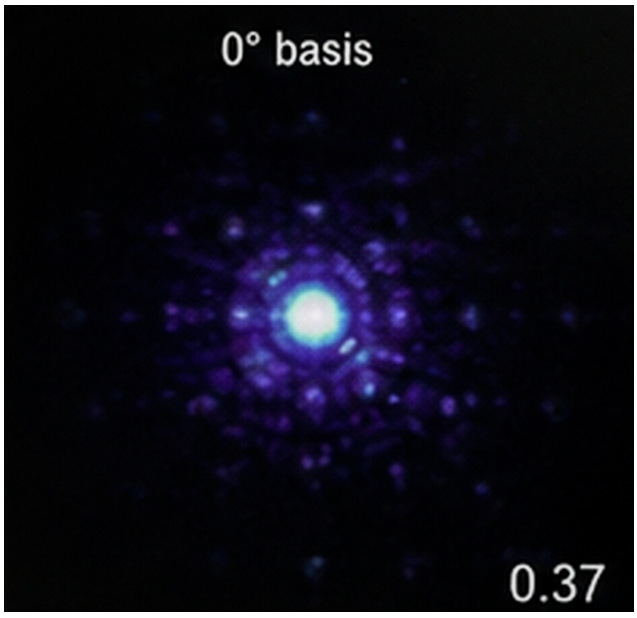

Figure 6. Unrotated $r = 3$ field.

In Figure 7, the field for $r = 3$ after rotation corresponds to the representation used by the control algorithm, wherein the estimated efficiency is improved from 0.37 to 0.42. This result confirms the applicability of using RMS mismatch as the screening criterion for commands. The relation similar to that introduced for Strehl ratio provides not a complete replacement for the diffraction analysis, yet allows the controller to have a handy criterion for identifying potentially valuable representations [34]. Accordingly, in the case $r = 3$, the

controller must not qualify the command as a low-efficiency one. The command should be considered recoverable if the application of rotated basis results in an increase in efficiency expectation exceeding the required margin. The above approach works conveniently in a range sensor design. In particular, a recoverable command may be applied in the current frame together with a rotated hologram.

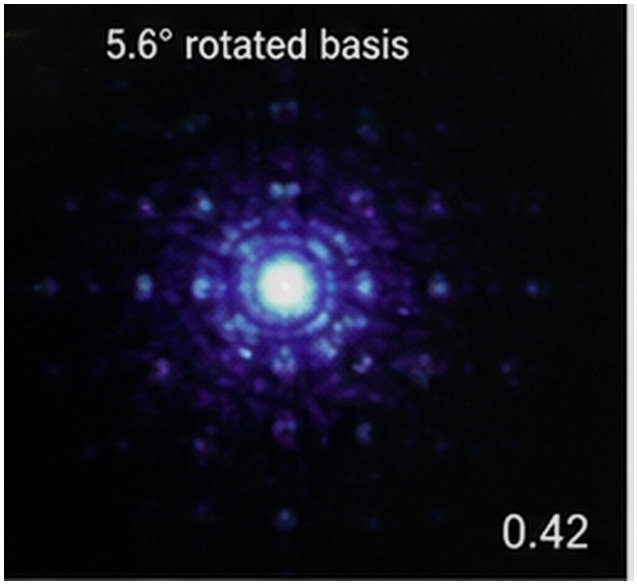

Figure 7. Rotated $r = 3$ field.

The absolute magnitude of the recovered efficiency is relatively small but large in terms of controllability. Even a five point increase of efficiency is significant because this implies the same quantity of usable light without any extra energy spent on the production of optical output from the laser. In a vast majority of optical systems this would represent an internal gain achieved by optimization of individual components, but here it was achieved with a proper choice of basis for the controller's work. This leads to new strategies. Instead of looking at the MEMS lattice as something that must be accepted and compensated for, the controller should consider it as a structure with a set of controllable freedoms. Storage of a relatively small angle rotation is much more cost effective than creation of larger aperture, employment of additional laser, or slowing down of the exposure sequence.

This achievement should be interpreted with caution. One successful recovery does not mean that all periods with low efficiencies are recoverable with rotations and that the maximum value of diffraction efficiency will always correspond to the optimal state of the MEMS. The modified configuration might have different far-field background, a new position for remaining diffraction orders, or an interference pattern interacting with the aperture stop. None of these changes negate the validity of the rotating technique but they mean that in order to achieve success, the ledger needs to record the results of using rotated states and then make its decision according to this information.

The output of rotation shows the restrictions inherent in geometrical steering alone. The same angle can have more than one corresponding digital value on the grid. If the control algorithm requires the one aligned along the axis, there might be unnecessary switching into a less optimal state. The recovered 13.5% proves that even a minor redefinition of the basis leads to better first-order efficiency locally. It is important in an industrial context as a less radical approach compared to modifying optics. The improvement is not only about having greater energy; what really counts is the more consistent ratio of command-to-delivered-power.

Two regions steering entails its own risks. Although the combined energy level might be sufficient for a pair of ROIs, the actual power transmitted to any particular one is insufficient for the task. In some cases, such as inspection or safety systems, equality of the sum total of

optical power does not ensure equality of measurement accuracy. The experiments in paired ROIs provide an interesting set of data. Symmetrical distribution creates a nearly equally efficient system. In case of the two asymmetrical arrangements, significant inefficiency in one branch prevails, as can be seen from [32].

Symmetric field from Figure 8 provides a well-balanced pair of regions. They have similar apparent size and intensity, which aligns with close values of branch efficiencies. This case serves as reference since there are no strong penalties to either branch due to both equal geometric locations and equal areas for power collection.

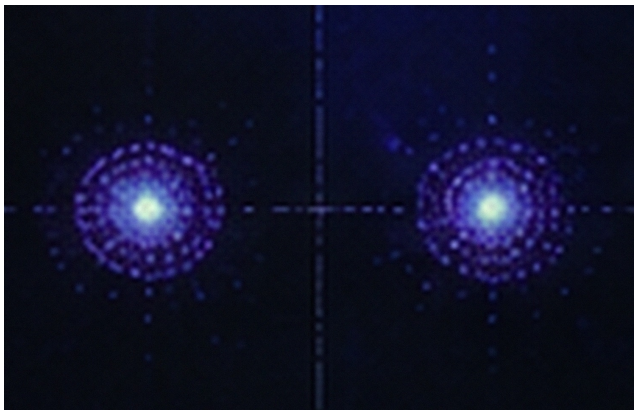

Figure 8. Symmetric two-ROI field.

Asymmetric equal-area field from Figure 9 illustrates why multi-region holograms' synthesis process should not take for granted equality of the received power by assuming equal areas of requested regions. Displacement of one branch makes it clearly less preferable as steering region, ROI 2 is noticeably worse in comparison with ROI 1. Therefore, control system accepting this command according to total efficiency will make a wrong conclusion.

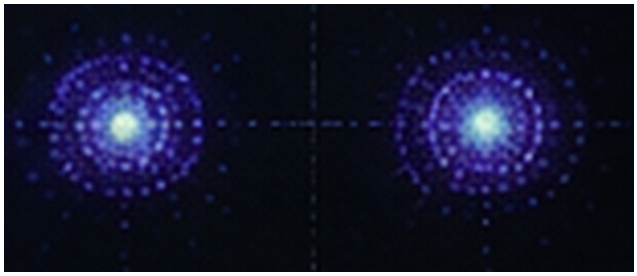

Figure 9. Asymmetric equal-area field.

Unequal areas in Figure 10 introduce an additional cause for branch variability since, besides the displacement, the target shapes are unequal in area. The reason why the authors consider branch equality a measurement is due to this example that shows asymmetrical shapes that do not protect the branch equality as seen in Figure 8. Figures 9 and 10 show asymmetrical shapes that endanger the branch equality.

From the values given in Table 2, it becomes clear that complex-field addition cannot resolve the branch-equity issue by itself. In the symmetric design, binary and complex-field approaches are both equally balanced, with only a small difference between the total efficiencies. In design (b), complex-field addition increases total efficiency from 0.2995 to 0.3023, but ROI 2 is still very low at 0.1275, whereas ROI 1 rises to 0.1748. In design (c), complex-field addition increases total efficiency from 0.2633 to 0.2712 and ROI 2 from 0.0992 to 0.1102, but the weaker branch gets a lot less energy compared to ROI 1. Therefore, complex-field addition is an important deterministic synthesis approach, but its unweighted version is insufficient to steer the branches equitably in asymmetrical designs.

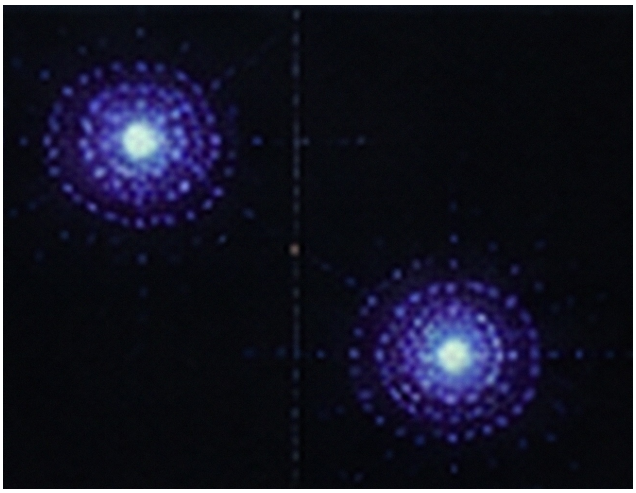

Figure 10. Asymmetric unequal-area field.

Table 2. Measured two-ROI diffraction efficiencies.

Layout	Binary π-phase grating			Complex-field addition		
	ROI 1	ROI 2	Total	ROI 1	ROI 2	Total
(a)	0.1641	0.1629	0.3270	0.1638	0.1600	0.3238
(b)	0.1710	0.1285	0.2995	0.1748	0.1275	0.3023
(c)	0.1641	0.0992	0.2633	0.1609	0.1102	0.2712

As seen from Figure 11, the first limitation in using paired commands becomes evident. Design (a) is almost perfectly balanced, but in the designs (b) and (c), ROI 2 becomes more inefficient even without discussing receiver gain or downstream processing of the received signals. This figure thus emphasizes once again the importance of the main point derived from the data presented in Table 2: optical energy is not the sole value influencing usefulness of a paired command.

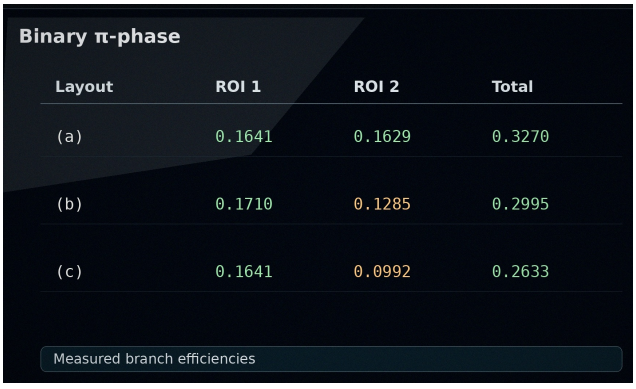

Figure 11. Binary branch efficiencies.

In Figure 12, we can see that despite the choice of the deterministic synthesis, the asymmetrical layouts exhibit unequal branch delivery. The numbers for layouts (b) and (c) need particular attention since ROI 2 still represents a weaker branch compared to the binary scheme even if the total efficiency is greater or equal to the binary method. That is why the later weighting is based on the parameters of branches.

The detailed analysis of the table with the pairs of regions provides the reason why the selection of the best synthesis method according to the overall efficiency does not solve the problem of branch inequality. The total of the complex-field method equals 0.3023 against the total of the binary method of 0.2995. Still, the weaker branch is only 0.1275. The

selection of methods should then be made in favor of the complex field, but the branches are unbalanced. In case (c), the complex-field method outperforms the binary scheme, both for overall efficiency and the weaker ROI, but the problem persists. What the conclusion drawn from all this information means is that the measured branches should be investigated prior to issuing a simultaneous control command.

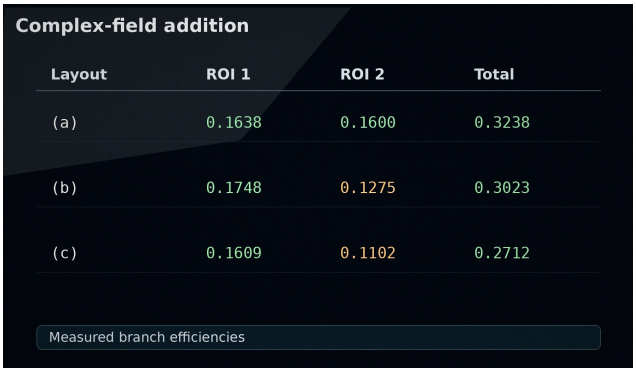

Figure 12. Complex-field branch efficiencies.

It matters for the purposes of testing of optical system performance. It should be clear by now that putting a power meter around the two spots and calculating the sum of power readings will not allow for certifying the simultaneous control command, since the measurement is inadequate to the equal priority sensing. The proper measurement procedure would involve computing the difference between the branches and comparing it with the task threshold. For robot safety, the threshold should represent the minimum value for obstacle recognition; in metrology applications, it would correspond to the signal-to-noise ratio necessary for edge localization, whereas for navigation, it would depend on the range update during the motion of the object.

This is where the imbalance factor I in Eq. (6) plays a role. With the complex-field model, the value for layout (a) would be $I = 0.0117$, which corresponds to a relatively balanced setup. In layouts (b) and (c), we get $I = 0.1565$ and $I = 0.1869$, respectively. Those are high enough numbers to make a difference since they imply that a significant part of the overall power advantage in delivery is in one branch. If both branches receive equal priority in the inspection process, the weaker one will have less signal margin or range confidence, as well as sensitivity to any background illumination. This means that the weighting scheme from Eq. (5) cannot just be considered an option.

The branch-equity indices in Table 3 transform experimentally-derived values into correction factors. For layout (a), little correction of the branch is needed as $\gamma = 1.012$, which is near unity. For layout (b), an amplitude buffer of 17.1% is required for ROI 2. For layout (c), an amplitude buffer of 20.8% is required for ROI 2. One must not interpret these correction factors as the post-correction efficiency of each branch, as the nonlinear interaction with phase-only weights may affect the total power available. Instead, these values should be understood as the initial deterministic correction based on experimental observations of branch asymmetry. In an operational controller, these corrections would be incorporated into the calibration ledger.

Table 3. Branch-equity indices from measured values.

Layout	$\eta_{\mathrm{bin,tot}}$	I_{bin}	$\eta_{\mathrm{cf,tot}}$	I_{cf}	Weaker branch	γ
(a)	0.3270	0.0037	0.3238	0.0117	ROI 2	1.012
(b)	0.2995	0.1419	0.3023	0.1565	ROI 2	1.171
(c)	0.2633	0.2465	0.2712	0.1869	ROI 2	1.208

Moreover, one can see from the above analysis that branch correction needs to be done on an illumination-level basis rather than using receiver-side gain only. While the latter helps

boost the overall signal, it does nothing about photons that were never sent to the target. A hologram weight attempts to equalize optical power prior to the interaction with a scene. This becomes especially important if the weaker branch is viewing a low-reflective surface or if the detector approaches the noise floor. The proposed method of optical weighting is a proactive correction, whereas receiver-side gain is just a compensating factor. Industrial application would need to implement both solutions simultaneously.

The comparison of the layouts (b) and (c) is especially telling. In layout (b), where the equal areas have no impact on protecting branch equality because of the asymmetric placement of the target. For layout (c), the unequal areas affect the efficiency, but improve the efficiency of the lower-performing branch through the addition of the complex field, yet this still does not eliminate the necessity for weightings. The implication is that steering using multiple regions will depend on more than simply allocating areas of equal size. Target geometry relative to each other, the combining rule of phases, and the phases' alphabetic order determine the power of the branches.

The operational difference between balanced and unbalanced steering illustrated in Figure 13 in the form of the correction display can be seen in the proximity of the former to the low-correction area and gradual increase in imbalance and buffer necessary for asymmetry correction. This trend is beneficial for the design of the controller due to the possibility of introducing a simple dispatching rule. Specifically, the control should handle low imbalance by itself, whereas moderate imbalance requires weighting before being handled. Finally, high imbalance paired with low total efficiency should be decomposed into two temporal shots. Again, this rule does not substitute the need for calibration per se, yet gives the industry a way to justify their approach to avoiding weak-branch failure.

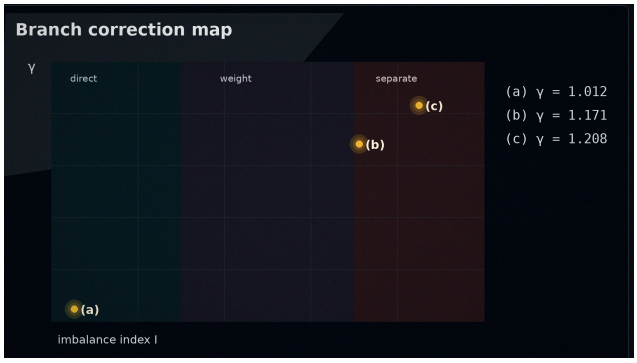

Figure 13. Branch correction display.

In addition, the study results confirm the importance of simultaneous consideration of the total efficiency and branch equity. If the controller aims at maximizing the total efficiency without regard to branch efficiency, then it might choose commands that maximize branch efficiency at the expense of other branches. On the other hand, if perfect equality is enforced by the controller, the overall optical efficiency drops below the margin for measurements. In turn, the calibration-conditioned approach sees steering control as a constrained allocation problem wherein the optical engine should provide sufficient power for measurement and allocate it as appropriate. It appears natural in light of the historical experience of solving problems in phase-only holography involving trade-offs among efficiency, uniformity, speckle, and computation costs [13,15,33]. The specific TI-PLM case allows for trade-offs to be done on the grounds of measurable efficiencies.

It follows that the multi-region system must not have the same steering policy across all possible region sets. For example, a single ROI in proximity to a dominant period will be issued without correction. In contrast, a single ROI near $r = 3$ must undergo rotated-basis testing to determine whether hologram generation is possible. For symmetric two ROIs, either the unweighted field technique or the binary technique will do if overall efficiency meets requirements. For asymmetric two ROIs, a weighted strategy must be used and evaluated against both overall efficiency and imbalance criteria. Otherwise, if the latter

criterion fails, separate branches are preferable because they can leverage their own periods and bases for generating holograms in the most suitable way for themselves. This is the key response offered by the numbers.

The numbers additionally imply that the apparatus should be calibrated according to the same terminology applied in control. Conventional optical calibration may provide a curve of diffraction efficiency as a function of period. This is essential but insufficient for the task at hand. Calibration is needed in the terms of the engine which must include a branch table for popular geometry pairs, a rotation table for weak periods, and a policy table which maps estimated efficiencies to dispatch options. As such, it will become important to keep the calibration ledger containing both optical and procedural entries. Optical entries will capture the measured efficiency, phase error, and branch power; procedural entries will determine dispatch modes as direct, rotated, weighted, split, or rejected.

The uncertainty must be addressed within the context of the controller as well. The values listed in Tables 2 and 3 are based on deterministic data for the corresponding conditions. The real world application would suffer from temperature changes, output variations of the laser, optical contamination, vibration, and changes in the reflectance of the target. It means that any realistic implementation should treat the values as nominal and leave sufficient margins for deviations from them. As an example, one must not equate a command with estimated efficiency slightly exceeding the threshold value with the command with a wide margin of tolerance. This information can be stored within the ledger together with the nominal expected efficiency using either some sort of a confidence interval or a derating factor. Even though no environmental data is included within the optical data set, the list of derived values allows including derating factors without modification of the synthesis formulas.

4. Industrial Application

Calibration-ledger control is most apparent in the context of a steering module integrated into the sensing workflow. For instance, a robotic inspection head can be required to light a weld seam, a fiducial mark, and a tip of a tool at various moments in time. An automated guided vehicle may need to switch its laser scanning range between long-distance tracking along aisles and close-in detection of obstacles. A dimensional metrology setup can be tasked with re-examining only several critical features with higher measurement accuracy without paying attention to other parts of the inspected object. As such, the optical command should be regarded not only as a desired direction but also as a place to make measurements. Such a scanning mechanism will be helpful for task-aware sensing, since it can offer transparency on its efficiency and the balance of its branches to the controller.

In regards to the industrial sensing application presented in Figure 14, it needs to be understood as the operating environment for the beam placement process and not as the application itself. Robotic inspection prioritizes exactness and repeatability, while AGV navigation prioritizes rapid revisits and range margin, and safety monitoring prioritizes weak branch robustness since the missed hazard zone may cost more than any small reduction in efficiency. Metrology prioritizes stable signal amplitude as reflectance/edge detection cannot be distinguished from steering-related optical loss. While these regimes share identical hardware, they place different priorities on total efficiency, balance, speed, and traceability. The calibration-ledger concept is important because it enables the TI-PLM engine to switch between different dispatch algorithms depending on the priority of the sensor operation.

Figure 14. Industrial multi-region LiDAR.

In terms of the safety monitoring case, the branch-equity consideration becomes especially relevant. It is beneficial to employ the simultaneous two-region command because it improves revisit rate. However, it might create a dead zone if the optical return from the weak branch drops under the margin of the detector, which is unlikely for the proposed 17.1% and 20.8% amplitude buffers. In the safety-rated application scenario, such commands would need to be de-rated unless post-calibration branch efficiency was measured. If this is not the case, then splitting the command into sequential operations is recommended. The steering engine should be allowed to split the command temporally if equal branch confidence is more important than simultaneous illumination.

The same result about period-efficiency applies to dimensional metrology. A measurement device which utilizes the amplitude of the signal as an indicator for surface properties or edge positions must avoid the confusion between steering dependent efficiency variations and the true sample variability. Weak periods around $r = 3$, 5.5, 6.5 and 7.5 can thus serve as calibrations points in the measuring sequence. One may also choose to rotate the data such that the efficiency is improved. The measured efficiencies can also be forwarded into the measuring sequence itself for correcting downstream effects. Such an approach improves transparency of measurements since the optical subsystem provides its own confidence rather than obscuring the effects of steering in the measurement signal.

In the context of mobile robotics and AGV navigation, the major benefit is provided through deterministic time behavior. An iterative hologram optimization scheme can be quite powerful; however, a navigation sensor must operate within strict boundaries with respect to the time needed to generate the commands from one frame to another. The control process is based on static equations, efficiency values and limited choices in rotations. It can be formulated into a deterministic command generation process. In particular, there is no need for solving the problem of global phase retrieval for each individual frame. It suffices to decode the command, refer to the ledger and apply the precomputed rotation or branch weights. If necessary, one may check the feasibility of simultaneous dispatching.

It also raises questions about the way TI-PLM modules should be specified. In general, one might expect pixel pitch, update rate, phase range, and maximum diffraction efficiency to be important parameters. However, for multi-regional LiDARs, these parameters are not enough. The following information should appear on an industrial module specification sheet: period-based efficiency graph; list of weak periods; rotated basis recovery table; branch balance results for several ROIs geometries. With this information, one could determine beforehand whether a module supports the desired pattern. It could also help in choosing the most conservative control strategy, if the optical task at hand was critical from either a safety or metrology standpoint.

4.1. Bounds on Measurements and Reproducibility

The numeric measurement is bounded by the optical conditions under which the TI-PLM characterization was made. This bound is significant since the variation between devices, the wavelength, the aperture stop, the size of the incident beam, the polarization state, the thermal environment, and relay optics may all affect the diffraction efficiency. The values presented in this paper are thus calibration data reflecting the specific behavior of the investigated TI-PLM and not universal constants valid for any MEMS phase modulator. An optical head ready for installation needs its own period map, list of rotations, and branch power before the rules for assigning ranges to sensing purposes come into play.

A second limitation is that the weighting algorithm assumes that the branch response can be adjusted using just an amplitude buffer while ignoring phase differences. This is indeed the case at first order, but a phase-only hologram formed from a weighted complex summation may redistribute energy non-linearly. The actual balance achieved after applying the weighting rule is thus expected to diverge from the one obtained using Eq. (5). The practical value of the expression lies in providing a reliable starting point. It tells the controller how much more weight should be placed on the weaker branch prior to tuning using a feedback loop. A commercial product would have its ledger include post-weighting

measurements of each branch while employing the theoretical buffer when no empirical data exists for a neighboring geometry.

The boundaries of rotation analysis are no less important. The recovery of a weak period from 0.37 to 0.42 by selecting a better basis suggests that the problem of a weak period can be solved by rotating the solution. However, one cannot claim that all weak periods have such a positive effect from rotation since in some cases rotation may worsen the problem by changing the phase-state sequence negatively. Consequently, each period's rotation result should be saved to avoid assuming that there is a universal solution to all weak periods.

One must provide an exact definition of what regions are considered when calculating multi-region efficiency. Efficiency calculations are affected by such factors as the integration window shape, background subtraction, and inclusion of diffraction artifacts outside the ROI area. Different researchers can thus produce inconsistent results when evaluating branch efficiencies even with the same hologram depending on the choice of the integration window. An example of the calibration ledger includes detailed information about the region of interest such as its size in terms of detector pixels or angles and whether the efficiency refers to the peak, integration or background-subtracted value.

Reproducibility necessitates the publication of both raw and derived data. Raw data includes single-period diffraction efficiencies, measured efficiencies per ROI branch, and basis-dependent recovery ratios. Derived data includes imbalance indexes, amplitude buffers, and dispatch categories. Failing to provide derived values would make it impossible for other scientists to test various balance tolerances or exposure theories, whereas failing to include raw data would hinder understanding of controller implications. In order to have a comprehensive TI-PLM steering experiment published, both types of data need to be reported to allow both optical scientists and control engineers to analyze the same dataset.

The calibration procedure may benefit from a number of extensions, leaving the core principle of control untouched. For instance, the measurements of branch efficiency may occur at a larger number of two-ROI separations and angles, thus turning the ledger into an interpolation surface rather than a table. Camera or detector readings in closed loop may automatically adjust branch weights upon variation of target geometry. Environmental derating is possible with measurements under temperature and vibration conditions. Deciding whether commands are simultaneous or separated in time is also possible using a task-level planner that analyzes the risks of weak-branch failure. However, all these modifications will simply increase deployment maturity, as the primary finding is that the optical command has to be filtered based on device properties.

5. Conclusion

Does TI-PLM multi-region steering work reliably as an industrial application for LiDAR? In particular, can such reliable hologram generation be governed through calibration instead of using geometrically ideal commands to control the steering modulator? The answer to this question is positive subject to the following condition. It becomes possible to steer the device beams to multiple regions under the control of calibrated holograms when the command dispatcher makes decisions based on period-indexed efficiency data, recovery tests, and branch equity weights. Without such a calibration layer in place, efficiency valleys and asymmetric ROI power deliveries cannot be predicted or mitigated.

The evidence to support this answer consists of four observations. First, because the TI-PLM mirror pitch is 10.8 µm, its nonlinear phase has 16 states. Consequently, steering periods must be characterized in terms of sampled phase values. Second, because of weak periods observed around $r = 3$, 5.5, 6.5, and 7.5, hologram commands are prone to cause period-specific inefficiencies. Third, the measurement of period $r = 3$ recovery from 0.37 to 0.42 demonstrates the possibility of recovering up to 13.5% relative efficiency by rotating the in-plane coordinate system. Fourth, the two-ROI measurement results show that it is possible to retain or enhance overall efficiency while maintaining insufficient power in ROI

2. The calculation of branch amplitude buffers, resulting in values of 17.1% and 20.8%, confirms this possibility and translates the branch inequity into control parameters.

Hence, TI-PLM beam steering has to be implemented as a calibrated optical control system. A stable industrial implementation will not only have to provide the holograms, but also keep track of conditions under which such holograms are acceptable to use. As a result, hologram commands may be issued when there is sufficient efficiency margin, rotated in case of low-efficiency weak period, weighted in case of inequality between simultaneous branches, and temporally separated in case of lack of branch equity or efficiency. The use of these commands allows one to employ MEMS phase-light modulation in industrial selective LiDARs, robotic inspection, safety and metrology applications in cases where optical power needs to be as precise as the steering angle. The former is especially critical when the optical output is used as a direct input for making the decision.

References

[1] McManamon, P. F., Bos, P. J., Escuti, M. J., Heikenfeld, J., Serati, S., Xie, H., & Watson, E. A. (2009). A review of phased array steering for narrow-band electrooptical systems. Proceedings of the IEEE, 97(6), 1078-1096.

[2] Behroozpour, B., Sandborn, P. A., Wu, M. C., & Boser, B. E. (2017). Lidar system architectures and circuits. IEEE Communications Magazine, 55(10), 135-142.

[3] Royo, S., & Ballesta-Garcia, M. (2019). An overview of lidar imaging systems for autonomous vehicles. Applied sciences, 9(19), 4093.

[4] Li, Y., & Ibanez-Guzman, J. (2020). Lidar for autonomous driving: The principles, challenges, and trends for automotive lidar and perception systems. IEEE Signal Processing Magazine, 37(4), 50-61.

[5] Senturia, S. D. (2001). Microsystem design. Boston, MA: Springer US.

[6] Judy, J. W. (2001). Microelectromechanical systems (MEMS): fabrication, design and applications. Smart materials and Structures, 10(6), 1115-1134.

[7] Lesem, L. B., Hirsch, P. M., & Jordan, J. A. (1969). The kinoform: a new wavefront reconstruction device. IBM Journal of Research and Development, 13(2), 150-155.

[8] Brown, B. R., & Lohmann, A. W. (1969). Computer-generated binary holograms. IBM Journal of research and Development, 13(2), 160-168.

[9] Ha¨ llstig, E., Sjo¨ qvist, L., & Lindgren, M. (2003). Intensity variations using a quantized spatial light modulator for nonmechanical beam steering. Optical Engineering, 42(3), 613-619.

[10] Goodman, J. W. (2005). Introduction to fourier optics, roberts & co. Publishers, Englewood, Colorado.

[11] Gerchberg, R. W. (1972). A practical algorithm for the determination of the phase from image and diffraction plane pictures. Optik, 35(2), 237-246.

[12] Fienup, J. R. (1980). Iterative method applied to image reconstruction and to computer-generated holograms. Optical Engineering, 19(3), 297-305.

[13] Fienup, J. R. (1982). Phase retrieval algorithms: a comparison. Applied optics, 21(15), 2758-2769.

[14] Reicherter, M., Haist, T., Wagemann, E. U., & Tiziani, H. J. (1999). Optical particle trapping with computer-generated holograms written on a liquid-crystal display. Optics letters, 24(9), 608-610.

[15] Curtis, J. E., Koss, B. A., & Grier, D. G. (2002). Dynamic holographic optical tweezers. Optics communications, 207(1-6), 169-175.

[16] Grier, D.G. A revolution in optical manipulation. *Nature* **2003**, *424*, 810–816.

[17] Maurer, C., Jesacher, A., Bernet, S., & Ritsch-Marte, M. (2011). What spatial light modulators can do for optical microscopy. Laser & Photonics Reviews, 5(1), 81-101.

[18] A Saleh, B. E., & Teich, M. C. (2007). Fundamentals of Photonics.

[19] Davis, J. A., Cottrell, D. M., Campos, J., Yzuel, M. J., & Moreno, I. (1999). Encoding amplitude information onto phase-only filters. Applied optics, 38(23), 5004-5013.

[20] Arrizón, V., Ruiz, U., Carrada, R., & González, L. A. (2007). Pixelated phase computer holograms for the accurate encoding of scalar complex fields. Journal of the Optical Society of America A, 24(11), 3500-3507.

[21] Hellman, B., Gin, A., Smith, B., Kim, Y. S., Chen, G., Winkler, P., ... & Takashima, Y. (2019). Wide-angle MEMS-based imaging lidar by decoupled scan axes. Applied Optics, 59(1), 28-37.

[22] Hellman, B., Luo, C., Chen, G., Rodriguez, J., Perkins, C., Park, J. H., & Takashima, Y. (2020). Single-chip holographic beam steering for lidar by a digital micromirror device with angular and spatial hybrid multiplexing. Optics Express, 28(15), 21993-22011.

[23] Azhar, E. A. (2018). Inorganic and Organic Photovoltaic Materials for Powering Electrochromic Systems (Doctoral dissertation, Arizona State University).

[24] Hutchison, D.N.; Sun, J.; Doylend, J.K.; Kumar, R.; Heck, J.; Kim, W.; Phare, C.T.; Feshali, A.; Rong, H. High-resolution aliasing-free optical beam steering. *Optica* **2016**, *3*, 887–890.

[25] Poulton, C. V., Yaacobi, A., Cole, D. B., Byrd, M. J., Raval, M., Vermeulen, D., & Watts, M. R. (2017). Coherent solid-state LIDAR with silicon photonic optical phased arrays. Optics letters, 42(20), 4091-4094.

[26] Komljenovic, T., Helkey, R., Coldren, L., & Bowers, J. E. (2017). Sparse aperiodic arrays for optical beam forming and LIDAR. Optics express, 25(3), 2511-2528.

[27] Hornbeck, L. (1995, January). Digital light processing and MEMS: Timely convergence for a bright future. In Storage and Retrieval For Image and Video Databases.

[28] Dudley, D., Duncan, W. M., & Slaughter, J. (2003, January). Emerging digital micromirror device (DMD) applications. In MOEMS display and imaging systems (Vol. 4985, pp. 14-25). SPIE.

[29] Bartlett, T. A., McDonald, W. C., & Hall, J. N. (2019, March). Adapting Texas Instruments DLP technology to demonstrate a phase spatial light modulator. In Emerging Digital Micromirror Device Based Systems and Applications XI (Vol. 10932, pp. 161-173). SPIE.

[30] Bartlett, T. A., McDonald, W. C., Hall, J. N., Oden, P. I., Doane, D., Ketchum, R. S., & Byrum, T. (2021). Recent advances in the development of the Texas Instruments phase-only microelectromechanical systems (MEMS) spatial light modulator. Emerging Digital Micromirror Device Based Systems and Applications XIII, 11698, 103-116.

[31] Ketchum, R. S., & Blanche, P. A. (2021, February). Diffraction efficiency characteristics for MEMS-based phase-only spatial light modulator with nonlinear phase distribution. In Photonics (Vol. 8, No. 3, p. 62). MDPI.

[32] Deng, X., Tang, C. I., Luo, C., & Takashima, Y. (2022). Diffraction efficiency of MEMS phase light modulator, TI-PLM, for quasi-continuous and multi-point beam steering. Micromachines, 13(6), 966.

[33] Pasienski, M., & DeMarco, B. (2008). A high-accuracy algorithm for designing arbitrary holographic atom traps. Optics express, 16(3), 2176-2190.

[34] Tyson, R. K., & Frazier, B. W. (2022). Principles of adaptive optics. CRC press.